UCRL-16650

University of California

Ernest O. Lawrence Radiation Laboratory

AN ABSOLUTE DETERMINATION OF THE EXTRINSIC AND INTRINSIC STACKING FAULT ENERGIES IN Ag-In ALLOYS

TWO-WEEK LOAN COPY

This is a Library Circulating Copy which may be borrowed for two weeks. For a personal retention copy, call Tech. Info. Division, Ext. 5545

Berkeley, California

DISCLAIMER

This document was prepared as an account of work sponsored by the United States Government. While this document is believed to contain correct information, neither the United States Government nor any agency thereof, nor the Regents of the University of California, nor any of their employees, makes any warranty, express or implied, or assumes any legal responsibility for the accuracy, completeness, or usefulness of any information, apparatus, product, or process disclosed, or represents that its use would not infringe privately owned rights. Reference herein to any specific commercial product, process, or service by its trade name, trademark, manufacturer, or otherwise, does not necessarily constitute or imply its endorsement, recommendation, or favoring by the United States Government or any agency thereof, or the Regents of the University of California. The views and opinions of authors expressed herein do not necessarily state or reflect those of the United States Government or any agency thereof or the Regents of the University of California.

Submitted to Acta Metallurgica

UCRL-16650

UNIVERSITY OF CALIFORNIA

Lawrence Radiation Laboratory
Berkeley, California

AEC Contract No. W-7405-eng-48

AN ABSOLUTE DETERMINATION OF THE EXTRINSIC AND INTRINSIC STACKING FAULT ENERGIES IN Ag-In ALLOYS

P. C. J. Gallagher

January, 1966

AN ABSOLUTE DETERMINATION OF THE EXTRINSIC AND INTRINSIC STACKING FAULT ENERGIES IN Ag-In ALLOYS

P. C. J. Gallagher

Inorganic Materials Research Division, Lawrence Radiation Laboratory, and Department of Mineral Technology, College of Engineering, University of California, Berkeley, California

January, 1966

ABSTRACT

Observations have been made of extrinsic-intrinsic node pairs, and of a hitherto unreported fault pair. It is shown that a simple extimate of the ratio of extrinsic to intrinsic stacking fault energy (γ_e/γ_i) cannot be made from the inscribed radii of node pairs, and that earlier qualitative results that $\gamma_e/\gamma_i > 2$, or more, are invalid.

The simple geometry of the new fault pair facilitates a straight forward absolute determination of both γ_e and γ_i. Contrary to published results, γ_e and γ_i have been found to be approximately equal. For the present alloys, $\gamma_e/\gamma_i = 1.09 \pm 0.1$ (for the electron-atom ratio e/a = 1.15) and $\gamma_e/\gamma_i = 1.03 \pm 0.1$ (for e/a = 1.23). Good absolute agreement has been obtained between γ_i determined from the fault pairs, and from the observation of extended three-fold nodes. It is concluded that extrinsic faults are rarely observed because of a high impedance to their formation arising from the co-operative glide which is necessary, but that once formed, the extrinsic fault energy is closely the same as the intrinsic.

I. INTRODUCTION

Previous work has shown that both intrinsic and extrinsic faults are present in f.c.c. alloys of low stacking fault energy. Estimates of the relative magnitudes of the intrinsic and extrinsic stacking fault energies (γ_i and γ_e respectively) have been made from examination of node pairs in Au-Sn [1] and Ag-Sn[2] and from a statistical treatment of the occurrence of stacking fault tetrahedra in Ni-70 At.% Co [3]. Only tentative conclusions could be reached, but the ratio of γ_e to γ_i was variously estimated as from 2 to 4.5 or more. Work by Booker and Brown [4] suggests that the result that $\gamma_e \sim \gamma_i$ in silicon [5] is spurious due to an anomalous diffraction effect.

In the present work silver-indium alloys have been examined in the electron microscope, their composition ranging from pure silver to Ag-12.5 wt.% In (electron-atom ratio, e/a = 1.23). Attention has been focused particularly upon the two alloys with lowest stacking fault energy (e/a = 1.15 and 1.23). The following section covers observations which have been made on extrinsic-intrinsic node pairs while subsequent sections describe an interesting new extrinsic-intrinsic fault configuration which provides a very advantageous method for determining the absolute magnitudes of both γ_e and γ_i.

II. INTRINSIC AND EXTRINSIC NODE PAIRS

Figure 1 shows a good example of an extrinsic-intrinsic node pair. Several reflections were used so that the Burgers' vector assignment (Fig. 1e) could be made with certainty. The notation used to describe

the Burgers' vectors is that of Thompson [6], and throughout this paper δ refers to the $(11\bar{1})$ plane, and BA = [011], CB = $[1\bar{1}0]$ and CA = [101].

Previous workers have drawn qualitative conclusions from fault configurations such as that in Fig. 1, by assuming that the ratio of the inscribed radius of one node to the other in the pair was approximately equal to the ratio of the extrinsic to the intrinsic stacking fault energy. This criterion applied to the node pair in Fig. 1 would suggest $\gamma_e/\gamma_i \sim 3$, but, as shown later, such a comparison is in fact invalid.

Figure 2a contains an extrinsic-intrinsic node pair in an alloy for which e/a = 1.10, and γ_i = 16 ergs/cm^2. A number of similar examples have been observed in this alloy. Figure 2b shows at A what is almost certainly a node pair in pure silver to which oxygen was added. Similar configurations have also been observed in pure silver, for which $\gamma_i \sim 20$ ergs/cm^2. Thus, the presence of extrinsic faults is by no means confined to materials of exceptionally low stacking fault energy.

Figure 3 contains a number of interesting features. The network in the central picture area contains only extended nodes establishing that intrinsic and extrinsic faulting has occurred. Further examples of extrinsic-intrinsic node pairs are indicated at points A, B, C, while extrinsic and intrinsic faults are also present at D, E and F. In several areas (e.g., F) an offset of the stacking fault fringes is noticeable where intrinsic and extrinsic faults are adjacent, as expected from contrast theory due to the phase shift of $2\pi/3$. It is emphasized that in these cases, as also throughout this paper, the extrinsic and

intrinsic faults share a common dislocation line, and that effects from overlapping faults do not arise. A comparison of Fig. 3a and b clearly reveals the presence of a cross-linking partial dislocation dividing the intrinsic and extrinsic faulted region for many of the node pairs. The presence of such a link is particularly clear in Fig. 3b at points A, B, D and F. The striking formation at point E, resembling an elongated node pair, is an example of the extrinsic-intrinsic fault configuration which is to be discussed in detail in the latter part of this paper.

Of the extrinsic-intrinsic node pairs in the figure, those at A and C each contain sensibly equal areas of extrinsic and intrinsic fault. By contrast, the node pairs at B and G consist of a considerably larger fraction of intrinsic fault. From Fig. 1, and particularly in Fig. 8, point P, we have evidence that the ratio of the inscribed radii in an intrinsic-extrinsic node pair can be as large as 5 or more, whereas in this same alloy previous work [7] has shown that for a sample of 40 single intrinsic nodes the standard deviation about the mean of a single measurement of the inscribed radius (w) was only $0.25\bar{w}$.

All the evidence points to the conclusion that the resultant configuration in an extended node pair depends very strongly upon factors other than the relative magnitudes of γ_e and γ_i. The evidence is substantiated by the results obtained in the latter part of this work.

The most important factor in determining the equilibrium configuration of the node pair is the elastic energy which results from the cross-over of the partial dislocations emerging from the extrinsically faulted node, particularly when γ_e and γ_i are small.

This elastic energy depends sensitively upon the angle at which the partials cross, since the repulsive force decreases markedly as the angle increases. Considerable distortion of the node pair is to be expected in cases for which the cross-over energy may thereby be reduced, especially when γ_e and γ_i are closely equal.

The observed shape of such pairs is in complete agreement with the above, in that the partials bounding the extrinsic fault are straight, or even have the reverse curvature to that found in intrinsic nodes, so as to maintain as large a cross-over angle as possible (c.f. Fig. 3, regions A, B, C, F, G).

Figure 4 illustrates three node pairs, for which let us consider that $\gamma_e = \gamma_i$, and that both are low. Without making detailed calculations it can be surmised that configuration (a) is unstable. By moving point C toward BB' (Fig. 4b) the total faulted area remains substantially the same, but the energy arising from the dislocation cross-overs at B and B' is reduced. For this reason too, the partials may take the reverse curvature in order to increase the angle of cross-over at points B and B', despite the increase in extrinsically faulted area which results. The formation of a resultant partial dislocation (CC' in Fig. 4c) also reduces the total energy for the same reason, despite the increased faulted area and dislocation line length.

We may conclude, therefore, that even for $\gamma_e = \gamma_i$ only in rare cases will a node pair contain equal areas of intrinsic and extrinsic fault. Although by no means intractable, the theoretical analysis of extrinsic-intrinsic node pair configurations would involve a careful

consideration of the character of each of the emerging dislocations, while, in addition, the network in region P (Fig. 8) clearly indicates that the constraints imposed by the surrounding dislocations are also of great importance.

It is concluded, therefore, that an examination of node pairs can lead to meaningful values of γ_i and γ_e only following a considerable expenditure of effort. The argument illustrated by Fig. 4 suggests that the extrinsically faulted area will almost invariably be smaller than one would expect from the relative magnitudes of γ_e and γ_i, due to the strong dislocation interactions involved.

III. EXTRINSIC-INTRINSIC FAULT PAIRS

The nature of the extrinsic-intrinsic fault pair at point E in Fig. 3 is most clearly appreciated from Fig. 3b. The observed magnitudes of d_i and d_e (defined in Fig. 5) vary in the same sense as the angle of projection is altered by tilting the specimen, establishing that the extrinsic and intrinsic faulted areas lie in the same plane.* It has been established from pictures under different diffracting conditions that the three long, sensibly parallel partial dislocations have the same Burgers' vector. Particular care has been taken to establish this fact without any doubt, and as many as 6 different reflections ($\bar{1}1\bar{1}$, $\bar{1}11$, 002, $2\bar{2}0$, $\bar{1}13$, $1\bar{1}3$) were used to photograph particular fault pairs.

---

*The configuration is not, of course, strictly co-planar, in that the dislocations lie on a pair of adjacent planes as is clear in Fig. 13. The configuration is planar in the sense that all the partial dislocations bounding the fault pair lie in the $(11\bar{1})$ plane.

Figure 5 illustrates the fault pair configuration diagramatically. The fault pair in Fig. 5 is lettered analogously to the node pair in Fig. 4c to emphasize that the fault pair is merely a node pair containing a cross linking dislocation which has been elongated in the direction defined by the unit vector $\underline{j}$ in Fig. 5. A number of advantages stem from the changes in geometry between the configurations of Figs. 4c and 5. With the notation of Fig. 5, these are listed below.

(1) For AA' >> AB the equilibrium separations d_e and d_i (of the partials bounding the extrinsic and intrinsic fault respectively) may be calculated simply by allowing for the repulsive forces between the dislocations BB', CC' and AA', and the attractive force which results from the faulted strips.

(2) The dislocations BB', CC' and AA' are parallel, have the same Burgers' vector, the same character (α), and lie in the same plane. Using isotropic elasticity theory a simpler theoretical relationship could not be hoped for, involving as it does only $\underline{b}$, α, γ_i, γ_e, d_i, d_e, ν and μ, where ν is Poisson's ratio, and μ the shear modulus.

(3) The simplicity of the configuration makes it possible for the first time in metals to calculate the stacking fault energy using anisotropic elasticity theory.

(4) The observer can discern whether a particular fault pair is suitable for measurement by the extent to which the three long partials are parallel.

(5) The measurements are not liable to error due to image displace-

ments which depend upon the diffracting conditions, since the three partials have identical b and α. The only correction in most cases is to allow for the inclination of the fault pair in the foil.

(6) As a consequence of the characteristic shape of the partials at the ends of the fault pair (discussed further below), the intrinsic and extrinsic parts of the pair may be identified from one bright field image.

(7) Within the range of stacking fault energies for which the fault pairs form, not only the relative, but the absolute magnitudes of γ_e and γ_i can be obtained with high accuracy (discussed further in a subsequent section).

In addition to their use in determining the stacking fault energy, fault pairs may also be important so far as the mechanical properties of the material are concerned in that subsequent glide in the plane containing the faults could be impeded. Figure 6 illustrates the interaction of a long screw dislocation with a number of other dislocations of different Burgers' vectors. The Burgers' vector assignment in Fig. 6c is readily accomplished from Figs. 6a and b; Fig. 6a, in particular, makes it clear that the long screw dislocation intersects the other dislocations, rather than curving away to the surface as one might conclude from Fig. 6b. [A number of anomalous contrast effects are contained in the figures in this paper; also in earlier work [1, 2]. These will be described below.]

It should be noted that the fault configuration illustrated in

Fig. 6c (and diagrammatically in Fig. 5) arises from the intersection of dislocations whose long range interaction is repulsive. A more detailed description of the formation process and the factors which favor it will be published shortly.

It is of interest to compare the fault pairs at B and C in Fig. 6b with the node pair at point D. The difference between the intrinsic and extrinsic faulted areas in the node pair is very marked, whereas the fault pairs (formed from dislocations with the same Burgers' vectors as the node pair) contain much more closely equal areas of extrinsic and intrinsic fault. At point A we have an example of a fault pair which, due to external constraints is not suitable for measurement. Only fault pairs with closely parallel partials have been measured, since the theory which will be used applies only to such cases.

Figure 7 illustrates complex intrinsic-extrinsic faults which are analysed in detail in Fig. 7e and f. While the faults are completely unsuitable for a determination of γ_e and γ_i the figure nevertheless contains very useful information. Once again, the lateral displacement of the stacking fault fringes makes it clear that intrinsic and extrinsic faults are present. It was suggested in the previous paragraph that fault pairs may represent a relatively sessile configuration. Nevertheless, a comparison of Fig. 7d with 7a shows that glide of complex intrinsic-extrinsic faults can take place, in this case simply as a result of heating due to the electron beam.

Confirmation of the assignment of identical Burgers' vectors to the long partials in a fault pair is evident in Fig. 7c taken with

the $\bar{2}20$ reflection. It has been found most convenient to measure the fault pairs photographed with the $\bar{2}20$ reflection so that only the partials are in contrast. The foil normal used for the majority of the pictures is [110], which means that $\bar{2}20$ is the only 220 type reflection available, and that one third of the fault pairs will have their long partials out of contrast (e.g., as in Fig. 7c). Fortunately good pictures have been obtained using the $1\bar{1}\bar{3}$ or $1\bar{1}3$ reflections by which means all three possible Burgers' vectors can be brought into contrast. Furthermore, as will be discussed below with reference to Fig. 10, as long as care is taken in recognizing which particular diffracting conditions are operative the fault pairs can also be measured when photographed with $1\bar{1}1$, $\bar{1}11$ or 002 reflections. Before going on to present the theoretical relationship between γ_i and γ_e, and the fault pair configuration, and the results which have been obtained from its application, the anomalous contrast effects are described.

IV. ANOMALOUS CONTRAST EFFECTS

Two types of anomalous effect have been observed--the first is that which is present in most of the photographs in this paper, and is particularly clearly visible for a number of diffracting conditions in Fig. 7a, b, d and Fig. 8a, b, c. It concerns the contrast observed at the central long partial, that which divides the extrinsic and intrinsic faulted areas. The same effect occurs for the crosslinking dislocation in node pairs, and may be seen in the previous work [1, 2] and in a large number of instances in Figs. 3 and 8 in the present work.

One expects, since all three long partials have the same Burgers' vector, that these three dislocations would be either in or out of contrast together. However, it is quite clear that this is not the case. In Figs. 7a, c and 8a a line of no contrast separates the intrinsic and extrinsic faults in all cases, except at Q in Fig. 8a. In all these cases (except Q) the outer two partials having the same Burgers' vector as the central partial (or cross-link in the case of node pairs) are in contrast.

In Figs. 7b and 8c the central partial (or cross-link in node pairs) is in contrast, while the outer partials are out of contrast (except at Q). These effects can be very confusing in making Burgers' vector assignments. The effects at Q are reversed from those elsewhere simply because the cross-linking dislocation has a different Burgers' vector from those in the other faults. One may state the general rules.

(1) A Shockley partial which would normally be in contrast for a given reflection appears out of contrast if it separates regions of extrinsic and intrinsic faulting which are also in contrast.

(2) Conversely, a Shockley partial which would normally be out of contrast for a given reflection appears in contrast if it separates regions of extrinsic and intrinsic faulting which are also in contrast.

Further examples of these effects can be seen in Fig. 3, and, of course, in Fig. 6b where the line of no contrast makes the dislocation appear not to cross. Detailed calculations on these effects are in

progress and will be reported at a later date.

The second anomalous effect is visible under diffracting conditions which show only the partial dislocations (i.e., $2\bar{2}0$, $1\bar{1}\bar{3}$ or $1\bar{1}3$ in the present work). In Fig. 8b there are numerous points, e.g., A, B, C, D, E, at which partial dislocations cross over one another at the join of an extrinsic to an intrinsic fault. Only at point A, however, is it clear that a crossover has occurred--in the other cases the contrast suggests, anomalously, that the dislocations remain parallel but do not cross.

A further particularly clear example of this is shown in Fig. 9. In both these bright field pictures the magnitude of s, the deviation from the Bragg position, was positive and close to that normally used for optimum contrast. In Fig. 9a with $g = 2\bar{2}0$, anomalous contrast is observed at points A and B where the partial dislocations do, in fact, cross over. With $g = \bar{2}20$ in Fig. 9b, the dislocation crossover at point A is now clearly visible, while the contrast at B remains anomalous. That similar dislocation interactions in closely adjacent sites should give different contrast indicates a very sensitive dependence upon the magnitude of s.

V. FAULT PAIRS, AND THE EXTRINSIC AND INTRINSIC STACKING FAULT ENERGY

5.1 Theory

In the present paper the theoretical treatment is limited to isotropic elasticity. More comprehensive experimental results are being obtained in order to test the predictions of anisotropic theory. The work of

Teutonico [8] provides a valuable basis for the necessary calculations.

With the notation of Fig. 5, the force between the parallel dislocations of character α is obtained by resolving the partial Burgers' vector $\underline{b}$ in the $\underline{j}$ and $\underline{k}$ directions. The repulsive force per unit length (F) between two dislocations distance d apart is thus

$$F = \frac{\mu b^2}{2\pi d}\left(\cos^2\alpha + \frac{\sin^2\alpha}{(1-\nu)}\right) \tag{1}$$

For the case of an infinitely long fault pair, the equilibrium configuration is described by the following equations.

$$\gamma_i = \frac{\mu b^2}{2\pi}\left(\frac{1}{d_i} + \frac{1}{(d_i + d_e)}\right)\left[\cos^2\alpha + \frac{\sin^2\alpha}{(1-\nu)}\right] \tag{2}$$

$$\gamma_e = \frac{\mu b^2}{2\pi}\left(\frac{1}{d_e} + \frac{1}{(d_i + d_e)}\right)\left[\cos^2\alpha + \frac{\sin^2\alpha}{(1-\nu)}\right] \tag{3}$$

We may also write

$$\gamma_e - \gamma_i = \frac{\mu b^2}{2\pi}\left(\frac{1}{d_e} - \frac{1}{d_i}\right)\left[\cos^2\alpha + \frac{\sin^2\alpha}{(1-\nu)}\right] \equiv \frac{\mu b^2}{2\pi}\left(\frac{1}{d_e} - \frac{1}{d_i}\right) f(\alpha) \tag{4}$$

The magnitude of $f(\alpha)$ varies from unity in the case of a screw fault ($\alpha = 0$), to $f(\alpha) = 1.92$ at $\alpha = 90°$ in the present alloys for which $\nu \sim 0.48$.

The extent to which Eqs. (2) and (3) are applicable to the observed fault pairs depends upon a number of factors. It is clearly desirable that the partials should be parallel and that the configuration should be as symmetrical as possible about a line parallel to $\underline{k}$ through the middle of the fault pair (c.f. Fig. 5). For a fault pair satisfying

these conditions, e.g. at B, Fig. 6, the main failing of Eqs. (2) and (3) is that their application will lead to an underestimate of γ_i and an overestimate of γ_e. The longer the fault pair, of course, the smaller is this discrepancy which arises from the strong forces involved in the dislocation crossovers at B and B'. Estimates of the accuracy of Eqs. (2) and (3) in their present application are made later in the text.

The most commonly observed fault pair configuration is that which at one end terminates in the foil surface. Numerous examples are contained in Fig. 8. Measurements have been made in the regions where the three partials are most nearly parallel, which is usually about one third of the way along the fault pair from the foil surface. Care must also be taken to avoid measuring fault pairs which are contained in a complex network of dislocations, e.g. at E in Fig. 8. It is interesting that in some, but not all of the fault pairs, the curvature of one of the long bounding partials changes suddenly locally, e.g. at E in Fig. 3, at C in Fig. 6b, and near C in Fig. 8b. This appears to arise from the presence of a strong local solute impedance.

A valuable aid in establishing the absolute accuracy of the determinations of γ_i and γ_e made from the fault pairs is a comparison with γ_i obtained from applying the recently published node theories [9-11] to the extended intrinsic nodes which have been observed. Particularly useful is an area such as that in Fig. 8 where good examples of nodes and fault pairs are in close proximity.

5.2 Experimental Results

The magnitudes of γ_i and γ_e have been determined from an examination of eleven fault pairs in the alloy with e/a = 1.15 and from

nine fault pairs in the alloy with e/a = 1.23. The correct Burgers' vector was readily assigned to the long partials in all cases so that the character of the fault pair, α, could be obtained. The foil normal unit vector, $\underline{n}$, was generally in the [110] direction. From trace analysis, using the 110 standard projection, the direction of the unit vector, $\underline{k}$, could be ascribed in terms of crystallographic indices applying the condition that it lies in the $(11\bar{1})$ plane. The measured values of d could thus be corrected for inclination in the foil since

$$d_{meas} = d \sin \phi, \quad \text{with } \cos \phi = \underline{k} \cdot \underline{n} \tag{5}$$

The maximum correction is by 22% corresponding to $\underline{k}$ in the [112] direction, while for $\underline{k}$ along $[1\bar{1}0]$, no correction is necessary.

The magnitude of d in the present work is in the range 250 to 400Å, giving rise to images 0.5 to 0.8 mm apart at the operative electron microscope magnification of 20,000X. Measurements have been made directly from the plates using both the Vanguard Motion Analyzer (which projects a magnified image on a screen, at 2.5X to 16X and cross wires read to 0.001 inch) and a microdensitometer. Excellent agreement was obtained between measurements on the two instruments (to better than 3%); the microdensitometer is to be preferred, however, as it completely eliminates any chance of subjectivity. In all the fault pairs examined it was possible to recognize the characteristic shape illustrated in Fig. 5. The partial dislocations bounding the ends of one part of the fault pair curve away gradually toward the long partial (intrinsic fault), while on the other side the end partials cross the

long partial as close to the fault pair as possible, and a constriction may frequently be seen (extrinsic fault). Dark field pictures have also been taken, and an established technique [12] for distinguishing between intrinsic and extrinsic faults has been followed to confirm that the assignments have, in fact, been made correctly.

Figure 10 contains microdensitometer traces from the traverse t in Fig. 8a, b, c. Similar sets of traces have been obtained from other faults which had been examined with a number of different reflections. It is clear from Fig. 10 why the $2\bar{2}0$ reflection has been preferred, since the position of the partials is readily measured. Diffracting conditions which lead to the outer partials in contrast, and the center one out (g either $1\bar{1}\bar{1}$, $1\bar{1}1$ or 002, depending on b) also enable d_e and d_i to be determined easily. In such cases a number of comparisons such as that of Fig. 10 show that the position of the outer partials under these reflecting conditions is where the intensity of the microdensitometer trace has dropped 20 ± 10% from its peak value. The intensity decreases so rapidly at the edges of the faults (see trace for g = $\bar{1}1\bar{1}$ in Fig. 10) that this uncertainty corresponds to an error of only ±3% in d. Less satisfactory measurements can be made when the outer partials are out of contrast, and measurements have not been made from such plates.

Table I contains the results of the measurements, and the values of γ_e and γ_i calculated therefrom using Eqs. (2) and (3). From the table we see that all the fault pairs had characters within 40° of pure screw. For both alloys we find that, contrary to earlier qualitative results, the ratio γ_e/γ_i is very close to unity. For the reasons

mentioned earlier it is possible that γ_e has been overestimated and γ_i underestimated by the application of Eqs. (2) and (3). In the following section two methods are employed to arrive at the magnitude of this effect, and a preliminary report is made of the effect of heat treatment on the fault pairs.

5.3 Checks on the Absolute Accuracy of γ_e and γ_i

A. Variation of d_i/d_e with ℓ/d_i

Figure 11 shows the variation of d_i/d_e with the ratio of the length of the center partial to the width of the intrinsic fault, ℓ/d_i. We know that when $\ell/d_i \to \infty$ the Eqs. (2) and (3) are completely valid in describing the fault pair. However, it is clear from Fig. 11 that even for relatively small values of ℓ/d_i the equations which have been used are a very good approximation. The influence of the forces arising from the end partials of the fault pair will cause a variation of d_i/d_e as a function of ℓ/d_i. From Fig. 11 we see that these forces have a negligible effect on the equilibrium value of d_i/d_e as long as $\ell/d_i \gtrsim 2$. Valid conclusions may therefore be drawn using Eqs. (2) and (3) even for short fault pairs, since the above condition, generally speaking, excludes only node pairs.

From the above we may conclude that the present measurements have led to very good absolute determinations of γ_e and γ_i.

B. Comparison with γ_i Calculated from Node Data

Table II compares the results obtained from measurements of the inscribed radius of extended intrinsic nodes with those from fault pairs. The node results have been calculated using the equations of Brown [9].

It has been shown [7] that for a given node configuration, applying the theory of Siems [10] leads to a value of $\gamma_i \sim 10\%$ less than after Brown, while the theory of Jøssang et al. [11] leads to a value of $\gamma_i \sim 20\%$ less than that calculated after Brown. A further uncertainty in the node theories arises from the term involving the cut-off radius of the dislocation core. A change by a factor of 2 in the magnitude of the core radius which is inserted in the equations alters γ_i by $\sim 10\%$.

Bearing in mind these uncertainties in calculations made from node data we see from Table II that the absolute magnitudes of γ_i determined from fault pairs are in rather good agreement with those obtained from nodes. This is particularly true for the alloy with e/a = 1.23, while even for e/a = 1.15 nodes and fault pairs in close proximity gave values of γ_i which agreed within 25%.

C. High Temperature Experiments

One further possibility which must be examined before concluding that the present results establish that $\gamma_e \sim \gamma_i$, is that preferential segregation may take place to the extrinsic fault. This would have the effect of reducing the apparent extrinsic stacking fault energy. That preferential segregation should occur seems unlikely since the atomic displacements differ only slightly for the two types of fault.

Figure 12 contains a sequence of pictures illustrating the appearance of extrinsic and intrinsic faults before, during and after an annealing treatment in the electron microscope. The offset of the stacking fault fringes is clearly visible establishing that both extrinsic and intrinsic faulting has occurred.

It is interesting to note that at room temperature prior to anneal wide bands of both extrinsic and intrinsic fault are present, probably due to the trailing partial being held up while the rest of the configuration continues to glide. Raising the temperature to 140°C is sufficient to activate movement of the partials, as shown in Fig. 12b, c. On cooling to room temperature, Fig. 12d, we find that the equilibrium configurations which have been reached are fault pairs for which d_i and d_i are closely equal.

The fact that in this case the same result has been obtained as for fault pairs observed at room temperature following room temperature deformation is strong evidence that preferential segregation does not occur.

It appears from sections 5.3, A, B, C that the values of γ_i, γ_e and γ_e/γ_i which have been obtained have absolute significance, Fig. 11 making it clear that Eqs. (2) and (3) are applicable without correction even to short fault pairs.

We are able to conclude, therefore, that the ratio of γ_i to γ_e in the present alloys is only slightly greater than unity, and there seems no reason to doubt that this result is of more general validity.

VI. DISCUSSION

Figure 13 illustrates the planar displacements which arise from the formation of an extrinsic-intrinsic pair, the configurations being those first described by Frank [14]. As pointed out by Frank and Nicholas [15] for both the extrinsic and intrinsic faults there are two

next nearest neighbor misfits of the type AA, BB or CC from which one expects the major part of the fault energy to be derived. Alternatively the intrinsic and extrinsic faults may be regarded as one and two layer twins respectively.

Throughout the earlier work on the nature of faults it was stated that no a priori reason could be seen to conclude which of the two types of fault would have the lower energy. The fact that extrinsic faulting has been relatively infrequently observed seems to be the main reason for the generally held view that the extrinsic stacking fault energy is higher than the intrinsic.

A more plausible explanation in the light of the present results is that generation of an extrinsic fault is difficult, but that once formed the fault energy per unit area is closely the same as for an intrinsic fault. In the latter respect the present experimental results are in accord with simple theoretical considerations in that the next nearest neighbor misfit energy is the same for both types of fault.

VII. SUMMARY

(1) Extrinsic-intrinsic node pairs are shown to be unsuitable for a straight forward determination of γ_e and γ_i.

(2) A new extrinsic-intrinsic fault configuration is described which possesses many advantages for the determination of γ_e and γ_i.

(3) In the two alloys examined, γ_e/γ_i has been determined as 1.03 ± 0.1, and 1.09 ± 0.1. Comparison of γ_i determined in this way with γ_i from node data indicates that satisfactory absolute determinations

of γ_i and γ_e can be obtained from the fault pairs, using the very simplest theoretical relations.

ACKNOWLEDGMENTS

Thanks are due to J. Washburn, P. Guyot and G. Thomas for useful discussions. The work was supported by the United States Atomic Energy Commission through the Inorganic Materials Research Division of the Lawrence Radiation Laboratory, University of California, Berkeley, California.

REFERENCES

1. M. H. Loretto, Phil Mag 10, 467, 1964
2. L. K. Ives and A. W. Ruff, J. Appl. Phys., in press.
3. M. H. Loretto, Phil Mag. 11, 125, 1965
4. G. R. Booker and L. M. Brown, Phil Mag., 11 1315, 1965
5. E. Aerts, P. Delavignette, R. Siems and S. Amelinckx, J. Appl. Phys. 33, 3078, 1962.
6. N. Thompson, Proc. Phys. Soc. B, 66, 481, 1953
7. P. C. J. Gallagher, J. Appl. Phys., in press
8. L. J. Teutonico, Acta Met., 11, 1283, 1963
9. L. M. Brown, Phil. Mag. 10, 44, 1964
10. R. Siems, Faraday Society, Discussion No. 38, p. 42, 1964.
11. T.Jøssang, M. J. Stowell, J. P. Hirth and J. Lothe, Acta Met. 13, 279, 1965
12. R. Gevers, A. Art, and S. Amelinckx, Phys. Stat. Sol., 9, 1563, 1963
13. A. W. Ruff, private communication, 1965
14. F. C. Frank, Phil Mag., 42, 809, 1951
15. F. C. Frank and J. F. Nicholas, Phil. Mag. 44, 1213, 1953

Table I

γ_e and γ_i from Fault Pair Data in Ag-In Alloys, e/a = 1.15 and 1.23

e/a = 1.15

$d_{ext.}$ (Å)	$d_{int.}$ (Å)	character, α (deg.)	f(α)
244	238	14	1.05
268	255	10	1.03
352	372	8	1.01
304	342	34	1.28
197	250	15	1.06
250	249	26	1.20
204	237	6	1.00
144	200	6	1.00
146	208	6	1.00
347	331	8	1.01
266	285	10	1.03

From which, with $\mu = 2.45.10^{11}$ dynes/cm^2, b = 1.67Å

$\gamma_{ext.} = 7.4 \pm 0.6$ ergs/cm^2. (deviation of single reading = ±1.8 ergs/cm^2)

$\gamma_{int.} = 6.8 \pm 0.4$ ergs/cm^2. (deviation of single reading = ±1.2 ergs/cm^2)

For e/a = 1.15, $\gamma_e/\gamma_i = 1.09 \pm 0.1$

e/a = 1.23

$d_{ext.}$ (Å)	$d_{int.}$ (Å)	character, α (deg.)	f(α)
395	393	23	1.15
351	417	14	1.06
510	511	6	0.99
375	390	9	1.02
409	589	38	1.35
375	370	30	1.22
511	454	34	1.30
325	325	24	1.15
452	450	17	1.08

With $\mu = 2.5.10^{11}$ dynes/cm^2, b = 1.67Å

$\gamma_{ext.} = 4.7 \pm 0.3$. (deviation of single reading = ±0.8 ergs/cm^2)

$\gamma_{int.} = 4.55 \pm 0.3$. (deviation of single reading = ±0.8 ergs/cm^2)

For e/a = 1.23, $\gamma_e/\gamma_i = 1.03 \pm 0.1$

Table II

Comparison of γ_i Determined from Fault Pairs, and from Isolated Intrinsic Nodes

		γ_i (ergs/cm^2)	Standard deviation of the mean (ergs/cm^2)	Standard deviation of a single reading (ergs/cm^2)
e/a = 1.23	Sample of 40 nodes [7]	5.55	0.3	1.3
	Nodes (3) close to fault pairs	4.8		
	Nodes in Ag-Sn (e/a = 1.23) [13]	4.9		
	Fault Pairs	4.55	0.3	0.8
e/a = 1.15	Sample of 25 nodes	10.0	0.5	2.0
	Nodes (4) close to fault pairs	9.2		
	Fault Pairs	6.8	0.4	1.2

FIGURE CAPTIONS

Figure 1 Burgers vector analysis of an extrinsic - intrinsic node pair in Ag-In (e/a = 1.23)

Figure 2 Extrinsic - intrinsic node pairs in a) Ag-In (e/a = 1.10) b) Ag + O_2 (4 ppm by vacuum technique)

Figure 3 Extrinsic and intrinsic node pairs, and fault pair (E) in Ag-In (e/a = 1.23)

Figure 4 Extrinsic - intrinsic node pair configurations, a) unstable, b), c) stable.

Figure 5 Extrinsic - intrinsic fault pair

Figure 6 a), b), Fault pairs in Ag-In (e/a = 1.15), c) Burgers vector assignment for fault pair B.

Figure 7 a), b), c), complex extrinsic - intrinsic faults, d) same after glide, e), f), Burgers vector assignments.

Figure 8 a), b), c) Examples of fault pairs in Ag-In (e/a = 1.23), d) analysis of lower fault pairs.

Figure 9 Anomalous contrast effects at partial dislocation cross-overs

Figure 10 Microdensitometer traces from traverse t in Fig. 8.

Figure 11 Illustrating the applicability of eqns 2) and 3) for $\ell/d_i > 2$, from the functional dependence of ℓ/d_i vs d_i/d_e.

Figure 12 The glide of partials bounding extrinsic - intrinsic fault pairs for the alloy with e/a = 1.23 a) at room temperature. b), c) at 140°C, d) subsequently at room temperature.

Figure 13 Description of an extrinsic - intrinsic fault pair in terms of atomic planes, illustrating the second nearest neighbor misfits.

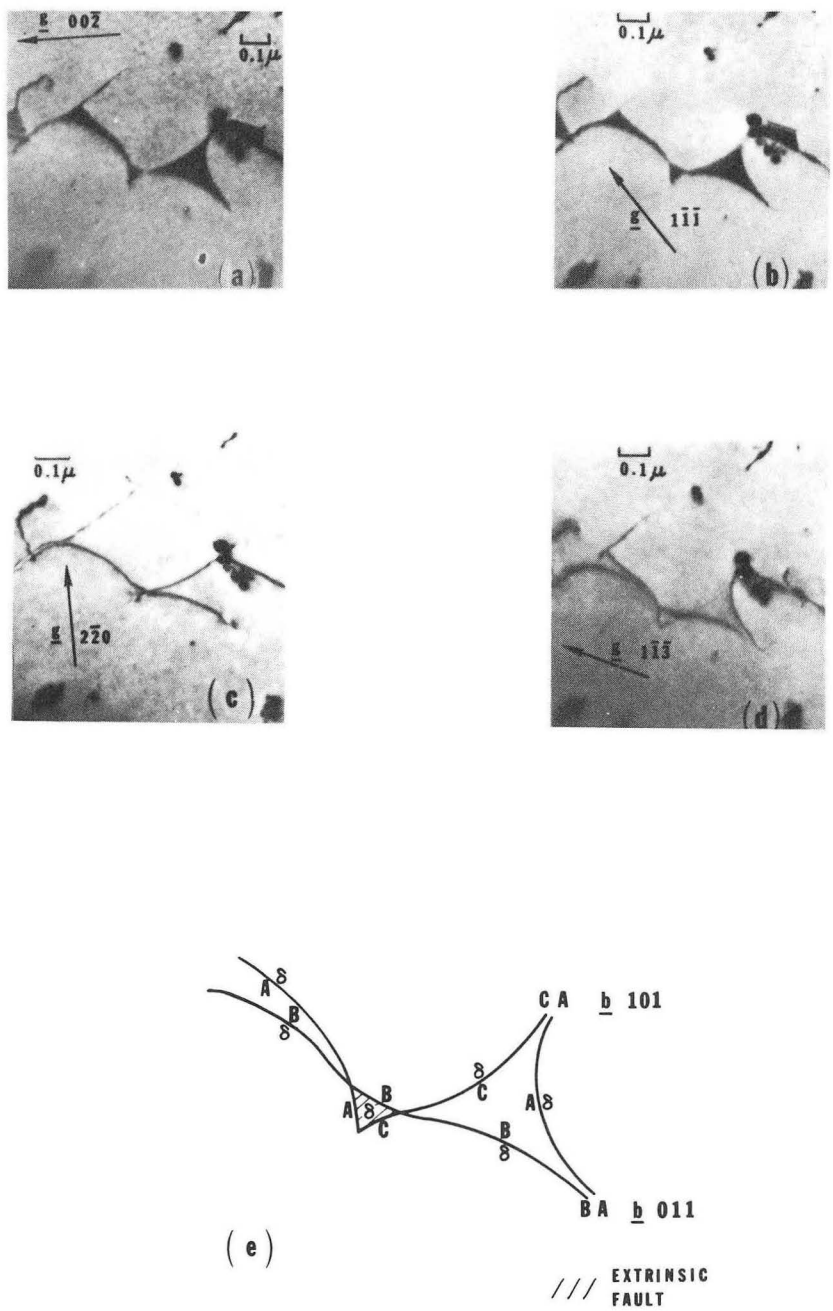
g 00$\bar{2}$
0.1μ
(a)
0.1μ
g 1$\bar{1}\bar{1}$
(b)
0.1μ
g 2$\bar{2}$0
(c)
0.1μ
g 1$\bar{1}\bar{3}$
(d)
A δ
B δ
A δ
B
C
δ
C
B δ
C A b 101
A δ
B A b 011
(e)
/// EXTRINSIC FAULT

ZN-5358

Fig. 1

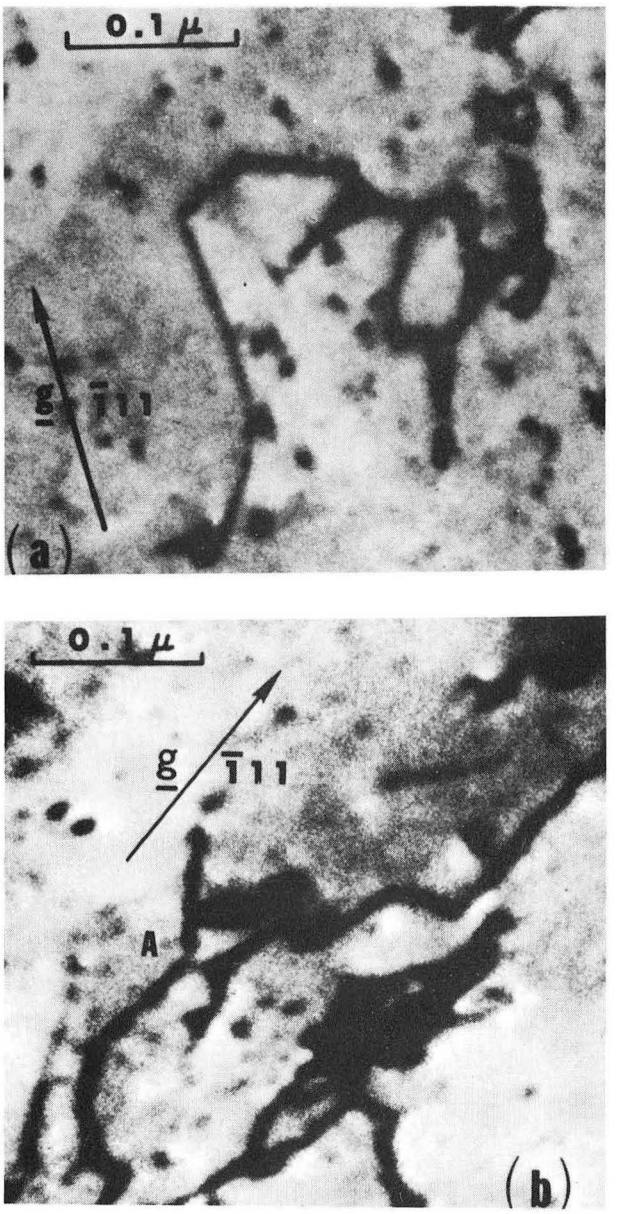

ZN-5355

Fig. 2

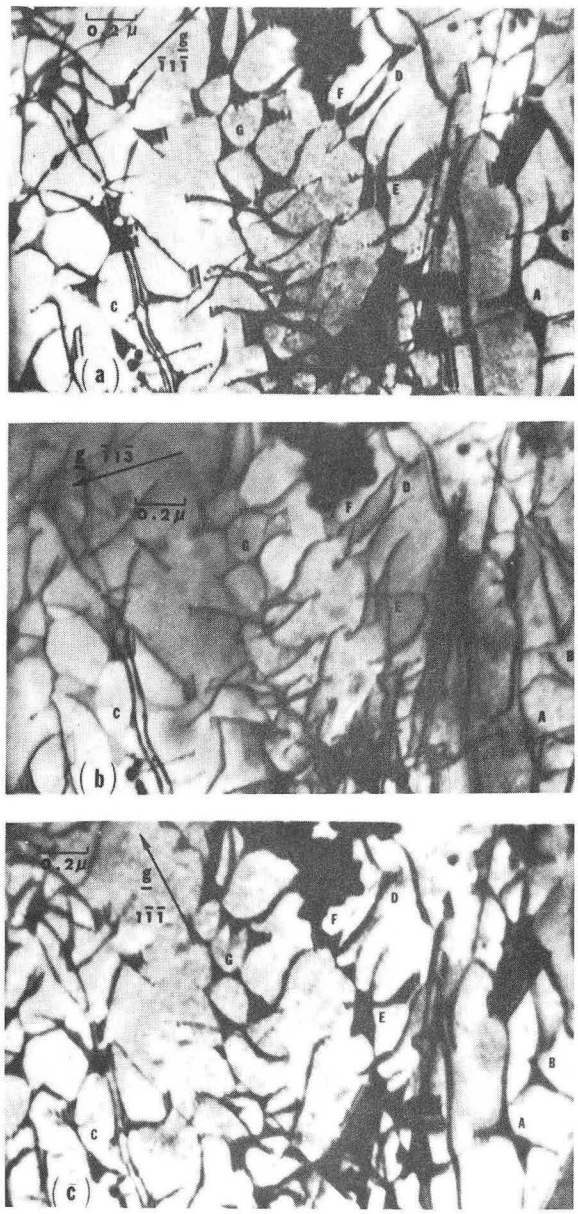
0.2μ
g
$\bar{1}11$
F
D
G
E
B
A
C
(a)
g $\bar{1}1\bar{3}$
0.2μ
F
D
G
E
B
A
C
(b)
0.2μ
g
$1\bar{1}\bar{1}$
F
D
G
E
B
A
C
(c)

ZN-5356

Fig. 3

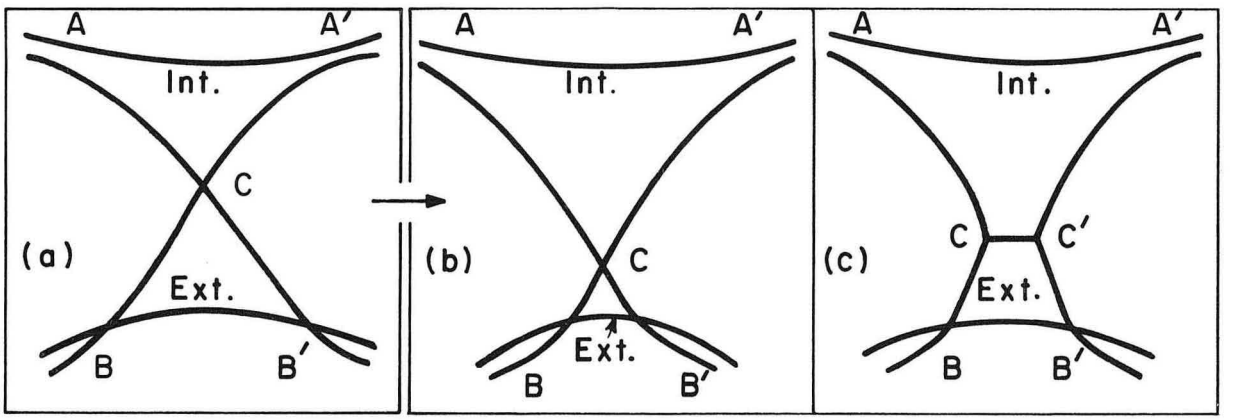

MUB-9203

Fig. 4

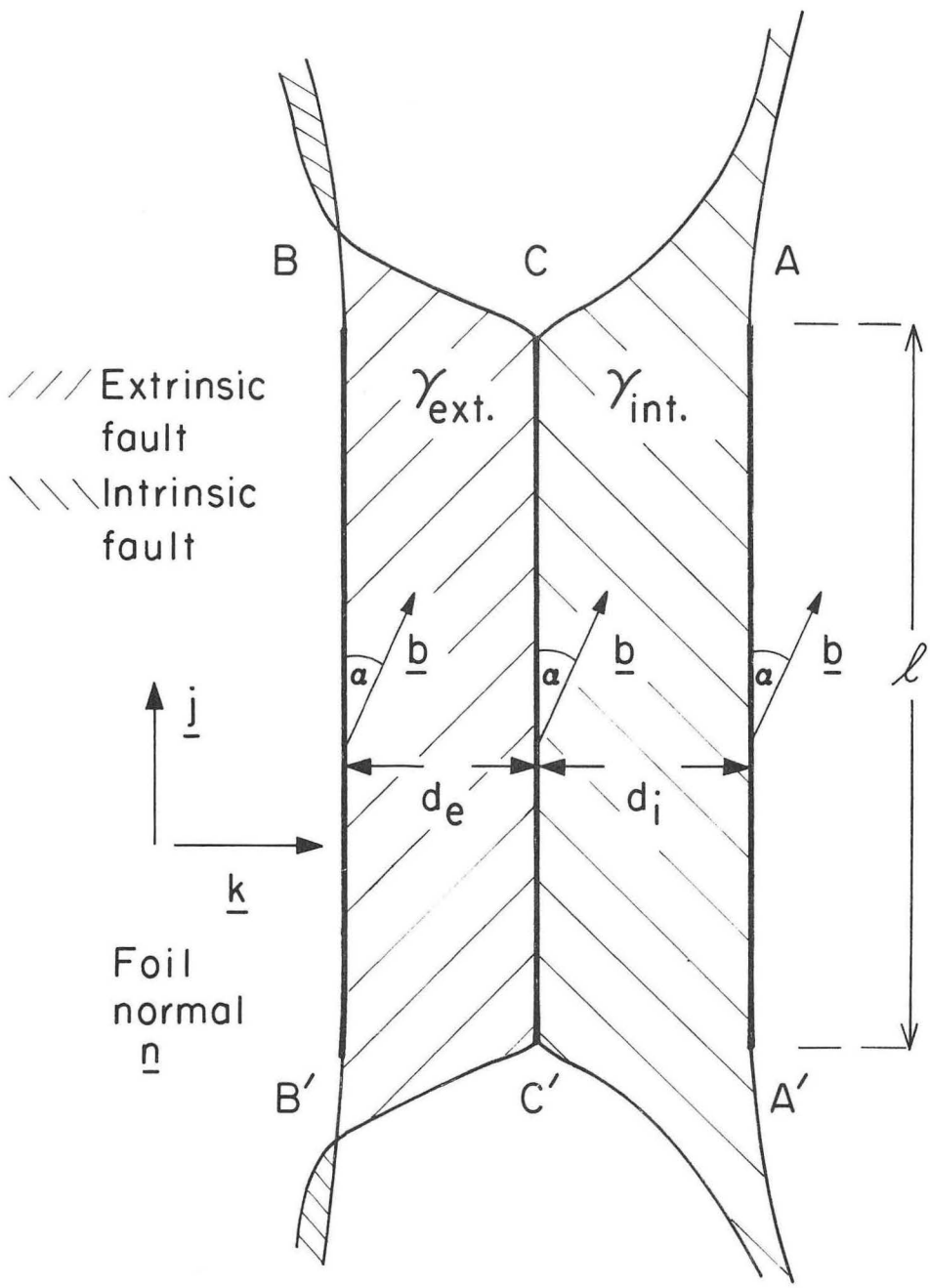

MUB-9206

Fig. 5

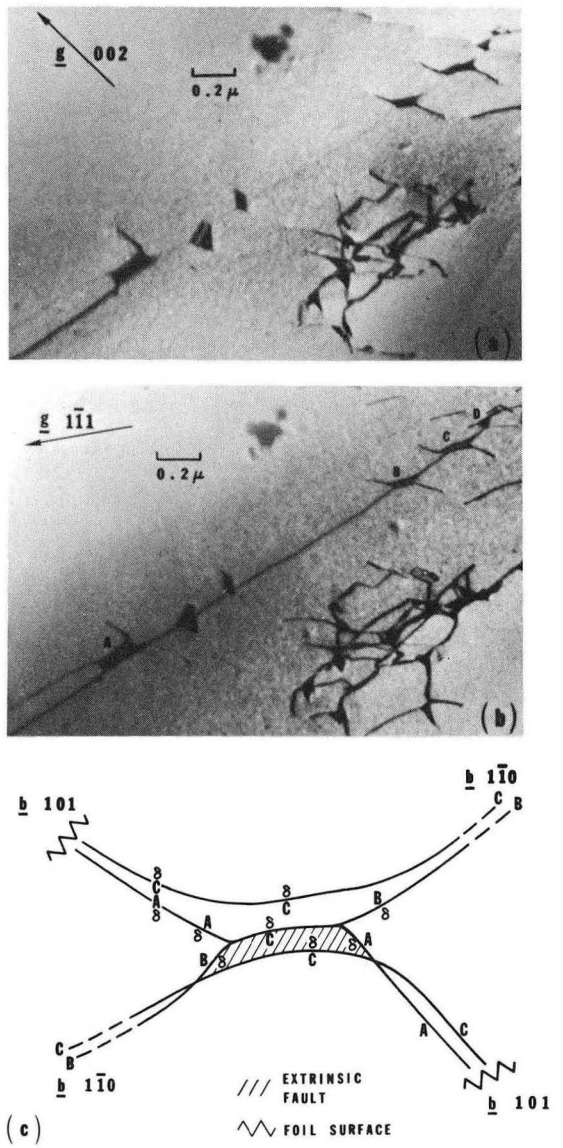
g 002
0.2μ
(a)
g 1$\bar{1}$1
0.2μ
(b)
b 101
b 1$\bar{1}$0
b 1$\bar{1}$0
b 101
EXTRINSIC FAULT
FOIL SURFACE
(c)

ZN-5354

Fig. 6

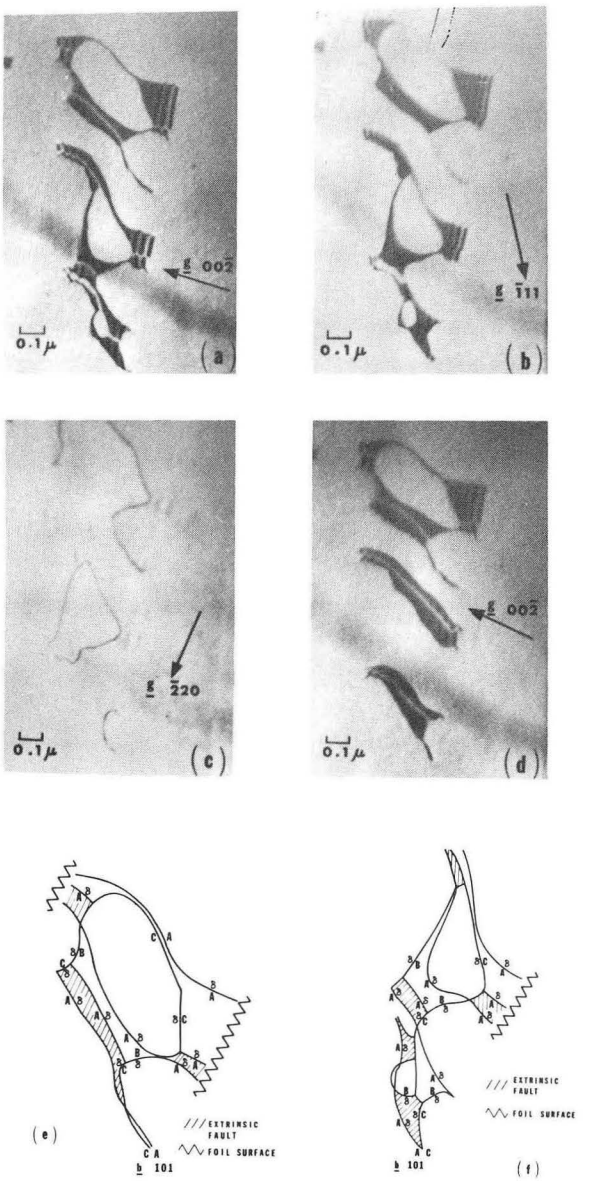
g 002̄
0.1μ
(a)
g 1̄11
0.1μ
(b)
g 1̄20
0.1μ
(c)
g 002̄
0.1μ
(d)
(e)
EXTRINSIC FAULT
FOIL SURFACE
b 101
(f)
EXTRINSIC FAULT
FOIL SURFACE
b 101

ZN-5353

Fig. 7

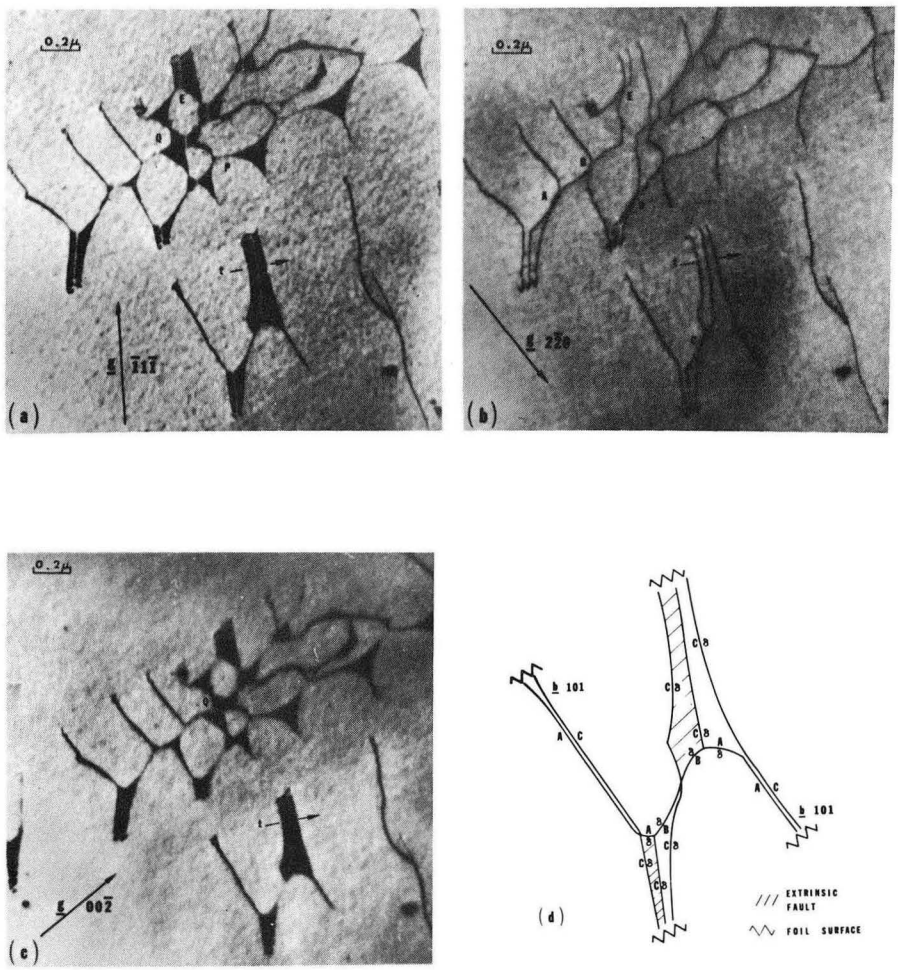

ZN-5357

Fig. 8

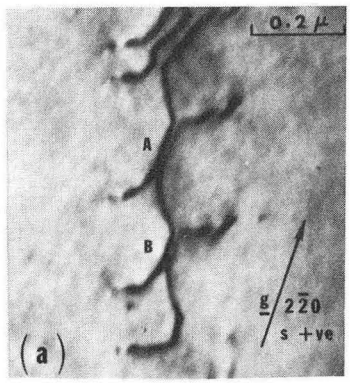

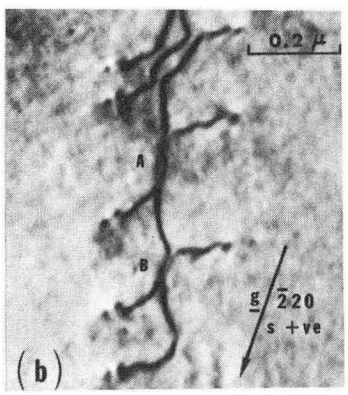

ZN-5360

Fig. 9

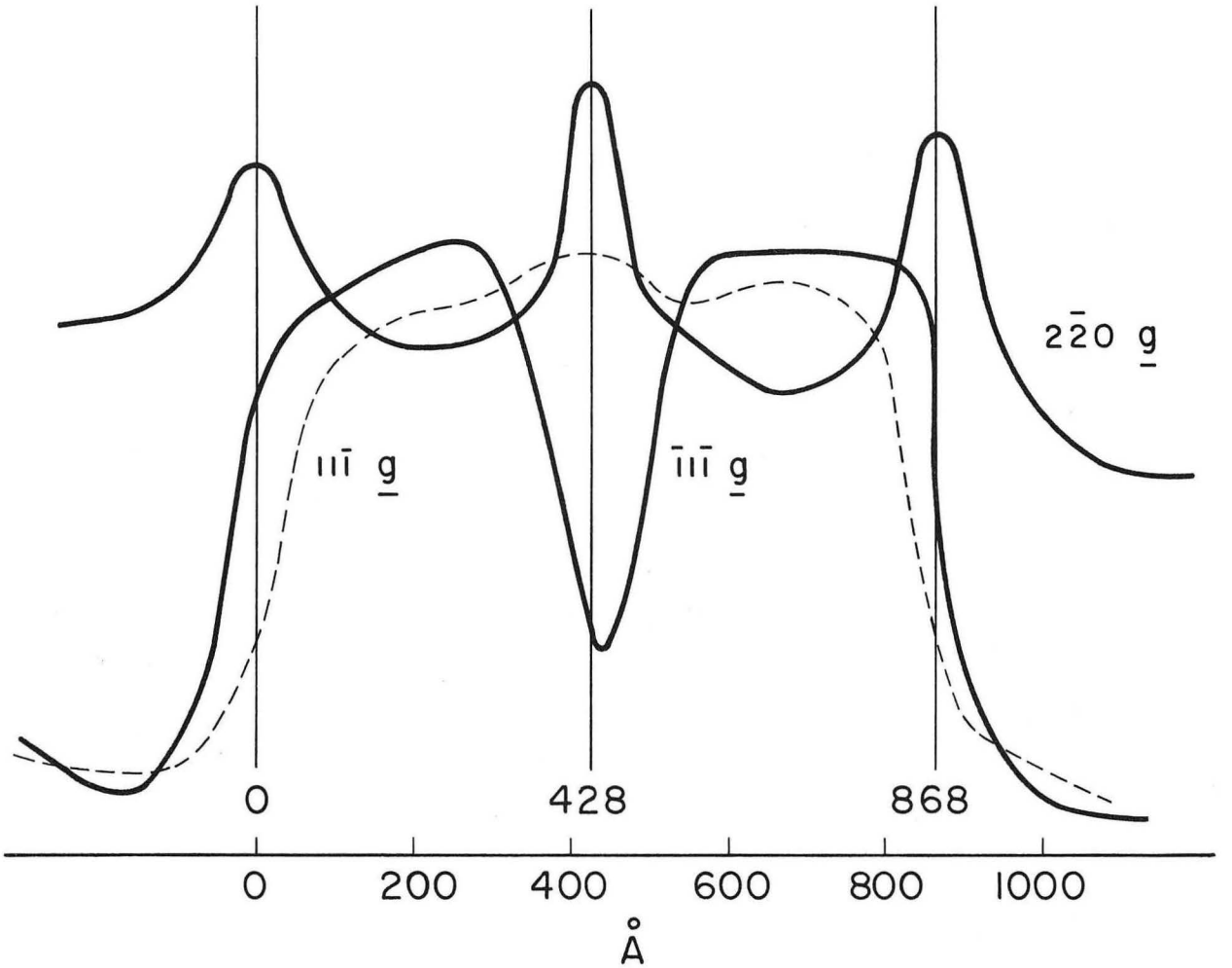

MUB-9202

Fig. 10

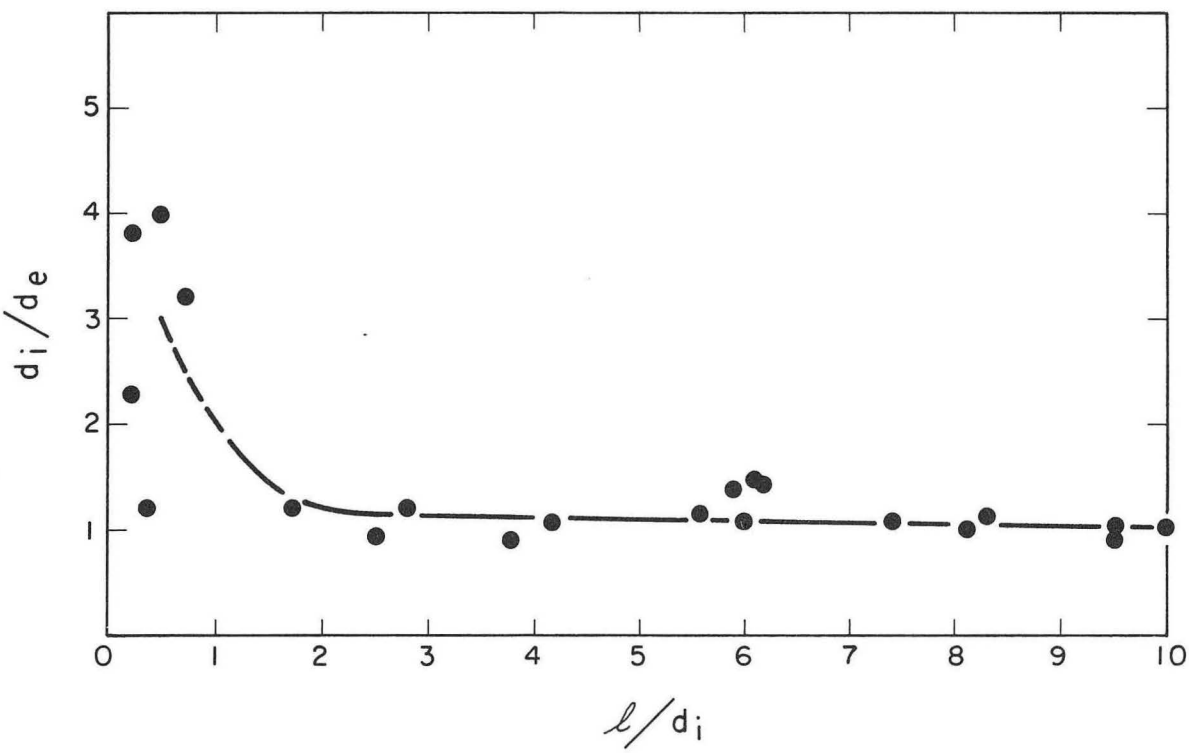

MUB-9205

Fig. 11

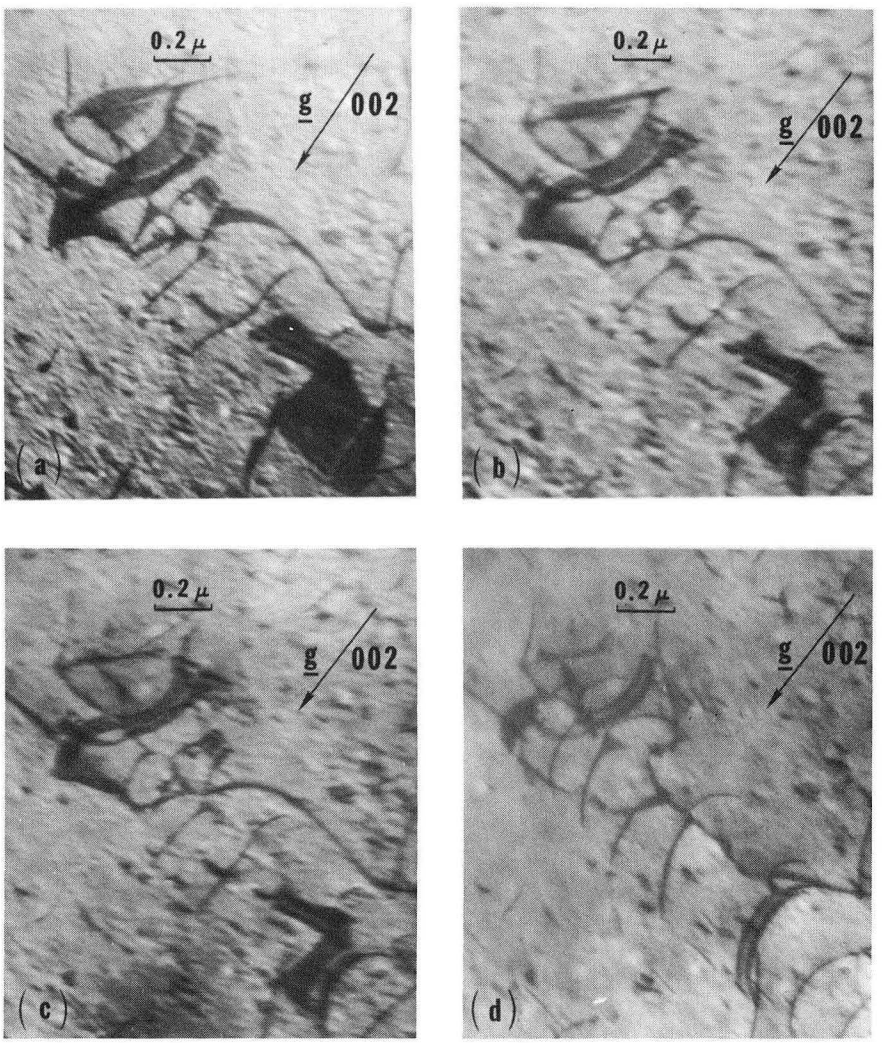

ZN-5359

Fig. 12

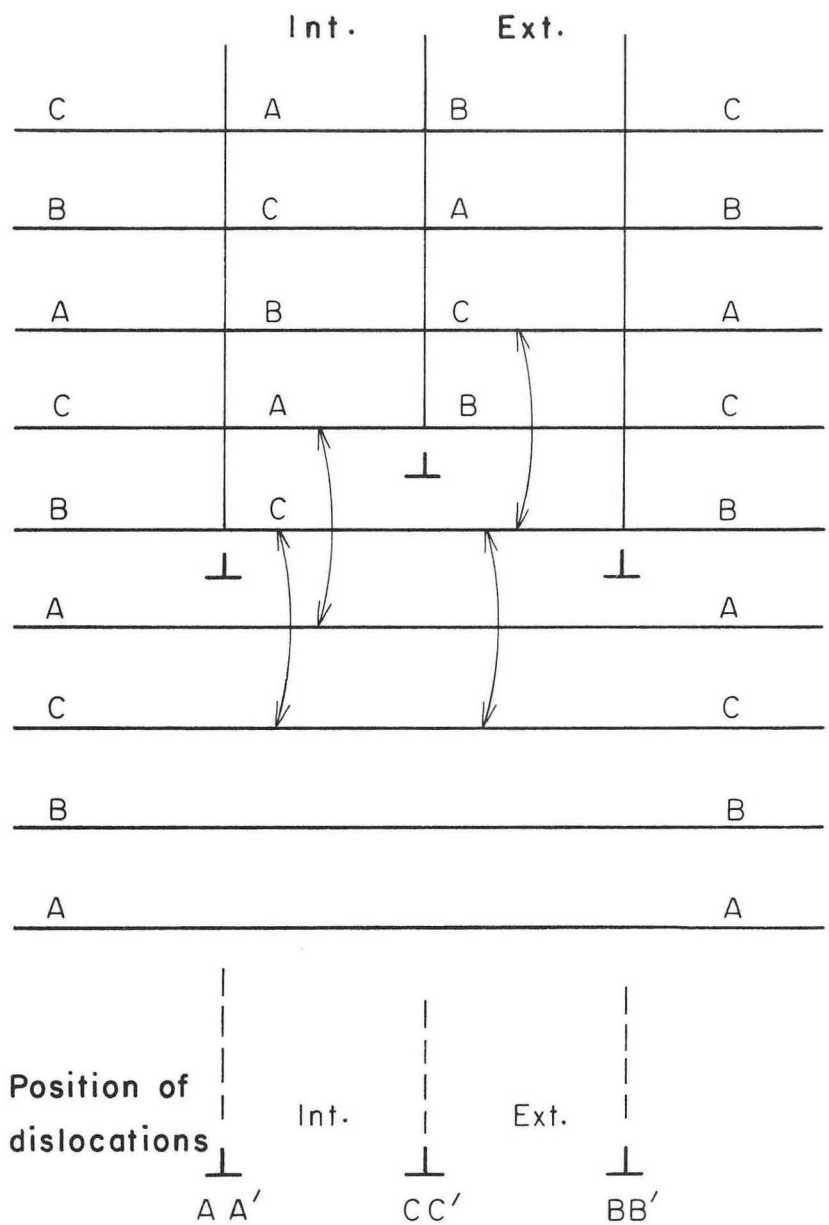

(Notation of figure 5)

MUB-9204

Fig. 13

This report was prepared as an account of Government sponsored work. Neither the United States, nor the Commission, nor any person acting on behalf of the Commission:

A. Makes any warranty or representation, expressed or implied, with respect to the accuracy, completeness, or usefulness of the information contained in this report, or that the use of any information, apparatus, method, or process disclosed in this report may not infringe privately owned rights; or

B. Assumes any liabilities with respect to the use of, or for damages resulting from the use of any information, apparatus, method, or process disclosed in this report.

As used in the above, "person acting on behalf of the Commission" includes any employee or contractor of the Commission, or employee of such contractor, to the extent that such employee or contractor of the Commission, or employee of such contractor prepares, disseminates, or provides access to, any information pursuant to his employment or contract with the Commission, or his employment with such contractor.